Bulletin of Engineering Geology and the Environment (2020) 79:2919–2935
https://doi.org/10.1007/s10064-020-01731-z

ORIGINAL PAPER

# Characteristics and main causes of earth fissures in northeastern Beijing Plain, China

Jiawei Wan [1,2] · Bin Li [1] · Chengxuan Tan [1] · Chengjun Feng [1] · Peng Zhang [1] · Bangshen Qi [3]

Received: 14 September 2019 / Accepted: 24 January 2020 / Published online: 11 February 2020


## Abstract

Earth fissures (EF) form in the northeastern Beijing Plain, causing horizontal and vertical displacements of the ground surface and damaging hundreds of buildings and roads. In addition, since 2009, an unprecedented number of cracks with vertical offsets have occurred in the Beijing Capital International Airport (BCIA), which is the busiest airport in China, causing serious financial losses and increasing the risk of air travel. The EF were divided into three groups, including EF1, EF2, and EF3, based on their distribution and deformation patterns. In general, the EF1 and EF2 fissures formed along segments of the NE-SW trending regional normal faults and have large vertical offsets but small widths. The deformation patterns, trenches and geophysical prospecting profiles, demonstrate that the EF1 and EF2 fissures propagated from the preexisting faults. In contrast, the EF3 fissures formed in a disorganized pattern above the paleochannels of the Chaobai River with short lengths and negligible vertical offsets. The monitoring data for the EF1 fissures indicates that the formation and deformation of the EF in the northeastern Beijing Plain were induced by groundwater pumping. The formation processes of the EF1, EF2, and EF3 fissures are classified into two categories: (1) on the existence of preexisting normal faults and (2) on the existence of paleochannels. Two hypothetical conceptual models are presented to illustrate the formation processes.

**Keywords** Earth fissures · Beijing · Preexisting fault · Paleochannel · Pumping

## Introduction

Earth fissures, also known as ground fissures, are a hazard created by geological dynamics and/or human forces. They can be liner or arcuate on the ground surface and vertical or inclined in the profiles. Earth fissures have been observed in hundreds of plains and basins worldwide, including in China, the USA, Mexico, Ethiopia, India, Iran, and Saudi Arabia (Ayalew et al. 2004; Al Fouzan and Dafalla 2013; Pacheco-Martínez et al. 2013; Conway 2015; Gaur et al. 2015; Peng et al. 2016; Nikbakhti et al. 2017). The formation of earth fissures is attributed to various factors, such as earthquakes, aseismic fault creep, overexploitation of groundwater, arid or semiarid climates, paleogeography, and special sedimentary textures and structures (Ayalew et al. 2004; Budhu and Adiyaman 2012; De Filippis et al. 2012; Zhang et al. 2015; Ghazifard et al. 2016; Hernandez-Marin et al. 2017; Chiaradonna et al. 2019; Xu et al. 2019).

The Beijing Plain is located in the northern part of the North China Plain and occupies approximately 40% of the land area of Beijing city (Fig. 1a). There is no detailed record of earth fissures before the occurrence of the Ms7.8 Tangshan

✉ Bin Li
libin1102@foxmail.com

Jiawei Wan
wjw2018@cugb.edu.cn

Chengxuan Tan
tanchengxuan@tom.com

Chengjun Feng
feng2010618@aliyun.com

Peng Zhang
zhangpeng0713@sina.com

Bangshen Qi
qibangshen@126.com

[1] Institute of Geomechanics, Chinese Academy of Geological Sciences, Beijing 10081, China

[2] China University of Geosciences, Beijing 100083, China

[3] Beijing Institute of Geo-exploration Technology, Beijing 100120, China

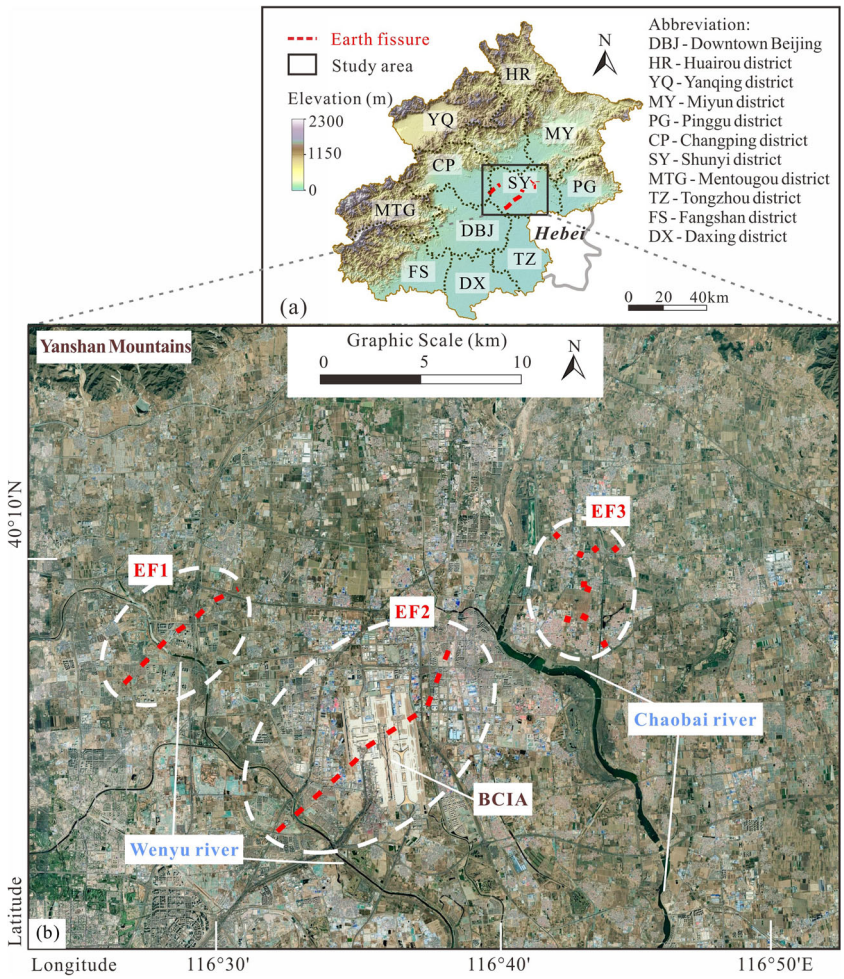


**Fig. 1** Maps showing the topography of Beijing city and the distribution of the earth fissures. **a** The topography of Beijing city and the distribution of the earth fissures. **b** The study area and the distribution of the earth fissures based on a satellite map from Google Earth

earthquake, on July 28, 1976, which occurred about 150 km from Beijing. The Tangshan earthquake directly and indirectly damaged or destroyed cities and induced numerous ground fractures in the Beijing Plain (Nábělek et al. 1987; Guo and Zhao 2018). The Changping, Shunyi, Fangshan, and Tongzhou districts were affected, especially along the Chaobai River (Beijing Hydrogeological and Engineering Geological Survey 2007, 2014).

After 1980, earth fissures formed more frequently, but without seismic activity, occurring synchronously with the rising demand on the water supply on the Beijing Plain where the citizens and public infrastructures are concentrated. The cracks unexpectedly emerged on buildings and roads with or without differential subsidence. At present, most of these earth fissures have been repaired or buried by artificial fill, so they cannot be observed or detected anymore. However, there is an exception on the northeastern Beijing Plain, which includes most of the Shunyi district and a small part of the Changping district and downtown Beijing (Fig. 1a).

The earth fissures in the northeastern Beijing Plain (EFBP) consist of three groups, the Gaoliying earth fissures (EF1), the Shunyi earth fissures (EF2), and the Nancai earth fissures (EF3) (Fig. 1b), all of which have caused serious financial losses and have elevated the disaster risk of Beijing city. According to our investigations, the majority of the EFBP fissures remain visible, and some are still propagating. Since 2009, the EF2 fissures have occurred in the middle of the Beijing Capital International Airport (BCIA), covering an area of about 0.12 $km^2$, nearly 10% of the airport has been affected.

At present, the main causes and formation processes of the EFBP fissures are not clearly understood despite several previous investigations performed by researchers and institutes. In addition, our works discovered that the scale of the EFBP fissures has expanded and there are many remarkable cracks have not been reported. In this paper, our findings and other researchers' studies were assembled to achieve a more comprehensive understanding of the EFBP fissures formation mechanism. Based on the results of features analysis and discussions of preexisting faults, paleochannel, and pumping, the respective roles of these factors in the formation of the three sets of earth fissures are discussed.

## Geological setting

From a tectonic perspective, the Beijing Plain is located in Cenozoic faulted basins, which evolved from the North China craton activating and splitting (Zhang et al. 2003; Yakubchuk 2009; Li and Santosh 2014; Pirajno and Santosh 2014). In the Quaternary period, the faulted basins in North China were covered by alluvial deposits accompanied by rapid tectonic subsidence, resulting in the preexisting faults being buried at depths of several meters to hundreds of meters (Foster et al. 2004; Qi and Yang 2010; Xu et al. 2019).

In the northeastern Beijing Plain, there are three buried regional normal faults, the Huang-Gao fault (HGF), the Shunyi fault (SYF), and the Sunhe fault (SHF), dislocated Quaternary sediments with N25°E-trending, N50°E-trending, and N50°W-trending, respectively. Significant differences in the thickness of the Quaternary sediments exist between the hanging wall and the footwall because the faults are dip-slip. Activities on the HGF, SYF, and SHF in Holocene period have been confirmed by Zhou et al. (2016), Zhang et al. (2016b), and Zhang et al. (2017), using magnetostratigraphy or palynostratigraphy methods. In addition, the accurate slip rate of the HGF in recent years (1985–2005) was determined by Jiao et al. (2005), using data from the Taoshan fault displacement observation site. The parameters and characteristics of the HGF, SYF, and SHF are shown in Table 1.

The study area is mostly flat with an altitude of 29–42 m above sea level, but it is lower in the south, except on the northern boundary of the Beijing Plain, i.e., the Yanshan Mountains. In the flat region, the thickness of the sediments is generally greater than 200 m with significant and sometimes sharp variations between the sides of the regional faults, which has been confirmed by drill-hole columns shown in Fig. 2. The sediments include coarse-grained materials, including alluvial sands and gravels, as well as fine-grained materials, including alluvial silts and silty clay. The coarse-grained materials are primarily located along the riverbeds and paleochannels of rivers, while the fine-grained materials are primarily distributed throughout the rest of the plain. The coarse-grained and fine-grained materials are interbedded and constitute the heterogeneous Quaternary aquifer system. The unconsolidated materials, which are mostly buried less than 50 m deep, form loose structures with high permeability as well as high compressibility, providing a favorable setting for seepage, erosion, and large soil deformations.

Beijing is one of the most water-stressed cities in the world with an absolute water shortage (McDonald et al. 2014). From 1958 to 1982, seven water supply plants and thousands of self-water supply wells were constructed to meet the enormous water demand of the increasing number of inhabitants. As a result of long-term large-scale groundwater exploitation, the groundwater table in the Beijing Plain has declined significantly since 1980, and the droughts in 1980–1984 and 1999–2011 caused the situation to deteriorate (Yang et al. 2011; Zhu et al. 2015).

In the northeastern Beijing Plain, the dynamic balance between groundwater exploitation, mostly from the Beijing 8th water plant, which was established along the Chaobai River in 1982 and extracts the most groundwater among all of the water plants in Beijing, and recharge, which is mostly from precipitation, was disrupted during the great droughts started in 1999. The groundwater levels declined sharply, which was observed in the monitoring wells of M1, M2, and M3 (Fig. 3). Because of the considerable reduction in groundwater storage, exploitation of the 8th water plant has been decreased annually. Currently, due to an increase in precipitation and a slight decrease in groundwater exploitation due to the utilization of reclaimed water and the transportation of water from the southern China, the descent of the groundwater table has been halted, and it has even started to rise, except in the vicinity of the well field (Fig. 3). In general, the groundwater depression cone has been maintained at depths of less than 50 m.

**Table 1** Geometric parameters, formation age, kinematics, and active characteristics of the HGF, the SYF, and the SHF

| Fault | HGF | SYF | SHF |
|---|---|---|---|
| Strike (°) | 25 | 50 | 310 |
| Dip direction (°) | 115 | 140 | 40 |
| Dip (°) | 80 | 60 | 65 |
| Length (km) | 132 | 100 | 80 |
| Formation age | Cretaceous-Neogene | Neogene-Quaternary | Neogene-Quaternary |
| Kinematics | Normal | Normal | Normal |
| Average slip rate (mm/year) | 0.77<br>(1985–2005 A.D.) | 0.62<br>(in Holocene) | 0.35<br>(in Holocene) |
| References | This paper and Jiao et al. 2005; Zhang et al. 2017; Zhou et al. 2016 | This paper and Zhang et al. 2016b | This paper and Zhang et al. 2017 |

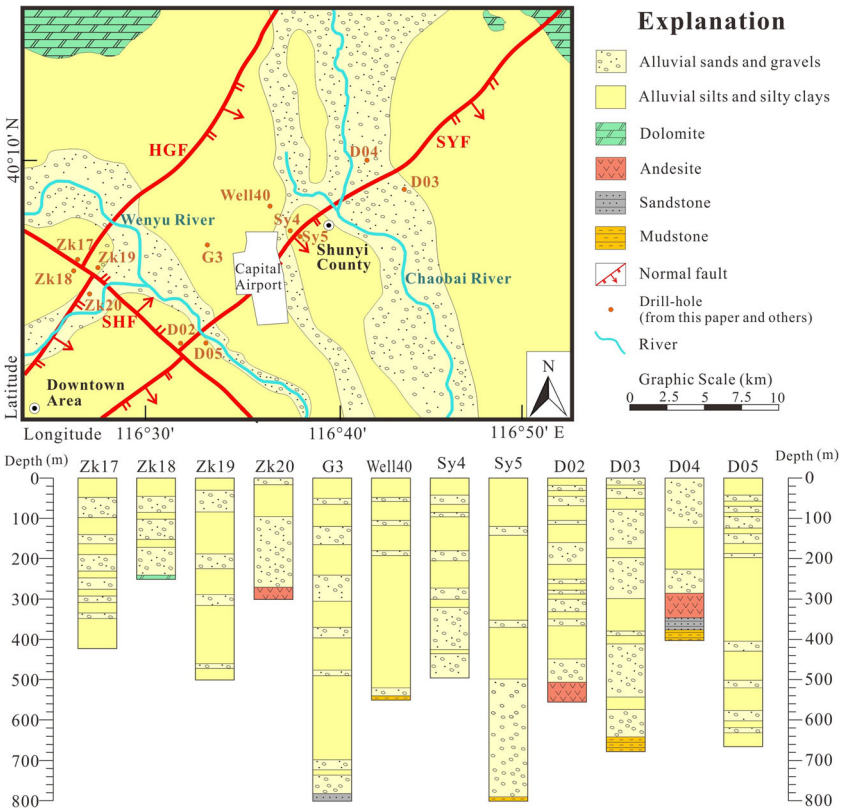


**Fig. 2** Geological map and drill-hole columns. The distribution and descriptions of the Quaternary sediments in the northeastern Beijing plain are shown. Descriptions of drill-holes Zk17, Zk18, Zk19, and Zk20 are from Zhang et al. 2017, that of G3 is from Zhou et al. 2016, those of Well40, Sy4, and Sy5 are from Zhang et al. 2005, and those of D02, D03, D04, and D05 are from this paper

## Characteristics and monitoring of the EF1 fissures

According to the Beijing Hydrogeological and Engineering Geological Survey (2007), the EF1 fissures were first observed in Xiwanglu village (Fig. 4), where several roads and houses were damaged by cracks and differential subsidence, in the 1990s. Tracing the direction, NE-SW, of the fissures extension, more damages were discovered subsequently in Tangzitou orchard, Tugou village (Fig. 5), and Baxian villas (Fig. 6) by this institue (Beijing Hydrogeological and Engineering Geological Survey 2007, 2014). All structures in the Tugou village have been demolished and removed entirely, and several houses in the Baxian villas, including villa 0702, are still blocked for further demolition, from our reinvestigation.

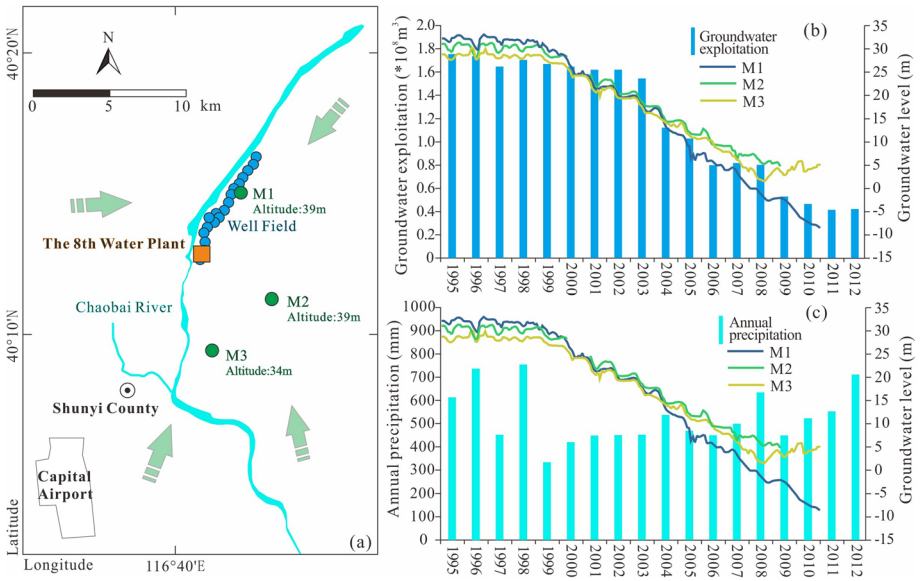


**Fig. 3** **a** Location of monitoring wells M1, M2, and M3, the well field, and the Beijing 8th water plant. The green arrows indicate the direction of the current groundwater flow. **b** Groundwater levels of wells M1, M2, and M3 and exploitation from the 8th water plant in 1995–2012. **c** Groundwater levels of wells M1, M2, and M3 and annual precipitation in 1995–2012. Groundwater levels are from Li et al. 2017, exploitation is from Zhang et al. 2016a, and annual precipitation is from Qin et al. 2018

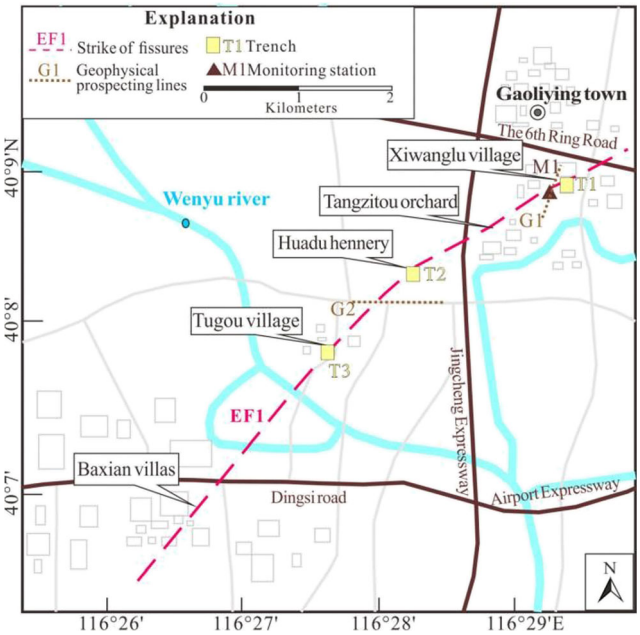


**Fig. 4** Location of the EF1 fissures and associated trenches, geophysical prospecting lines and monitoring station (assembled from the Beijing Hydrogeological and Engineering Geological Survey 2007; Wang et al. 2013; Lu et al. 2014; Zhang et al. 2016c)

The EF1 fissures strike NE-SW and extend for almost 7 km, although statistically (Table 2) the EF1 fissures are comprised of discontinuous fissures with angular deviations. With few exceptions, the EF1 fissures have small widths but larger vertical dislocations; therefore, the buildings and roads crossed by the fissures subside or collapse. The Beijing Hydrogeological and Engineering Geological Survey (2014) discovered another land deformation pattern, in the Tangzitou orchard where a 90-m-long, 5~10-cm-wide fissure emerged on the ground surface with a vertical dislocation of less than 4 cm. The relative broadening was probably due to surface erosion by rainfall.

**Fig. 5** Damaged building and floor in Tugou village (derived from the Beijing Hydrogeological and Engineering Geological Survey 2007). Location is shown in Fig. 4. The lens is aimed at north, and the right side has subsided

**Fig. 6** Damaged roads and Villa 0702 in the Baxian villas (derived from the Beijing Hydrogeological and Engineering Geological Survey 2014). Location is shown in Fig. 4. Southeastern side has subsided

A trench was excavated in Xiwanglu village by the Beijing Hydrogeological and Engineering Geological Survey (2007) to explore the geometric features of the EF1 fissures at shallow depth. The trench was 20-m long, 9-m wide, and 8.4-m deep, part of it is shown in Fig. 7. The trench revealed that 6 layers of sediments and 1 layer of fill were dislocated by a fracture plane, which was marked with gray paint, strikes N70°E and dips southeast. Along the fracture plane, the hanging wall subsided, and the upper buildings were damaged. Layers L5 and L6 were deposited in 18.8 ± 0.9 ka-21.1 ± 0.5 ka B.P., according to the Beijing Hydrogeological and Engineering Geological Survey (2007), and were denuded on the footwall before the L7 fill deposited. It indicates that the southeastern side of the EF1 fissure slipped downward along a preexisting fracture plane over time before the occurrence of modern human activity. Accordingly, the EF1 fissure in Xiwanglu village was supposed to be an extension of the HGF because of the substantial consistence. Similar structures were explored by Zhang et al. (2016c) in Huadu hennery and by Lu et al. (2014) in Tugou village.

The Beijing Hydrogeological and Engineering Geological Survey (2007, 2014) and Zhang et al. (2016c) arranged geophysical prospecting lines in Xiwanglu village and Tugou village, applying techniques such as shallow seismic exploration, multielectrode resistivity method, and ground-penetrating radar (GPR). Their results verified the connection between the EF1 fissures and the regional normal fault HGF.

Wang et al. (2013) and the Beijing Hydrogeological and Engineering Geological Survey (2014) set an automatic monitoring system and an artificial observation network, respectively, both in the Xiwanglu monitoring station (Fig. 4), in order to observe any dynamic changes in the EF1 fissure deformation. Their data and graphs showing that the hanging wall of the EF1 fissure has subsided continuously, from

**Table 2** Statistics for the EF1 fissures (derived from the Beijing Hydrogeological and Engineering Geological Survey 2007, 2014)

| Location of EF1 | Strike | Length (m) | Width (cm) | Vertical dislocation (cm) |
|---|---|---|---|---|
| Xiwanglu village | N60 °~75 °E | 400 | < 4 | 1~19 |
| Tangzitou orchard | N60 °~71 °E | 90 | < 10 | 1~4 |
| Huadu hennery | N8 °~39 °E | 300 | < 3 | 1~19 |
| Tugou village | N20 °~53 °E | 200 | < 5 | 1~15 |
| Baxian villas | N30 °~40 °E | 600 | < 5 | 1~10 |

2009 to 2012, which is in accordance with the HGF movement mode in the Quaternary period. But it is much faster, given the average slip rate 0.77 mm/year of the HGF (shown in Table 1).

The Beijing Hydrogeological and Engineering Geological Survey (2014) set up an artificial observation network that adopted leveling in thirteen observation points to simultaneously detect the absolute vertical displacement on opposite sides of the EF1 fissures, monthly. The location of each point, relative to the EF1 fissure, is shown in Fig. 8a. From 2010 to 2012, twelve annual displacement data sets show increasing uplift on the footwall and decreasing subsidence on the hanging wall (Fig. 8b). This alleviated the land subsidence but extended the duration and deterioration of the earth fissure due to the entirely different displacement direction. The uplift of the footwall and the subsidence delay of the hanging wall may be related to the end of a drought that lasted for over 10 years and the resultant groundwater recovery, which started in 2011.

According to Wang et al. (2013), the automatic monitoring system employed three displacement sensors on the hanging wall and one datum on the footwall to monitor the three-dimensional deformation of the EF1 fissure, which included recording data every half hour. Figure 9a shows that the subsidence occupied the first place, the opening followed, and the right-lateral shear is the least. The proportion of these three modes of cumulative displacement was 28.35: 15.18: 6.10, from August 1, 2009 to November 1, 2012. The fluctuation in the horizontal displacement curves and the substantial decline in the vertical displacement curves indicate the dominant position of the subsidence. Figure 9b and Fig. 9c present similar variation tendencies, indicating that the hanging wall deformed horizontally along two basically fixed orientations, primarily south and occasionally north, based on the N70°E strike of the EF1 fissure in Xiwanglu village and the ratio between cumulative horizontal displacements. Figure 9d shows the delay in the land subsidence over the years, which is in agreement with the leveling observations (Fig. 8b). It also shows a sharp change from declines in April to June (or May to July) to almost constant levels in the other months. The conversion was not explained by Wang et al. (2013) but is speculated to be associated with heavy pumping of groundwater after winter ended in this paper.

## Characteristics of the EF2 fissures

The EF2 fissures were first discovered by the Beijing Hydrogeological and Engineering Geological Survey (2007, 2014) in five workshops and one boiler room in the Beijing 2nd rubber plant in 1985. The records indicate that the southeastern side of the EF2 fissures subsided and the fissures propagated striking NE-SW rapidly. The affected buildings and roads have been reinforced and repaired repeatedly, yet all of these efforts were in vain, and the damages have continued to increase since the earth fissures propagated.

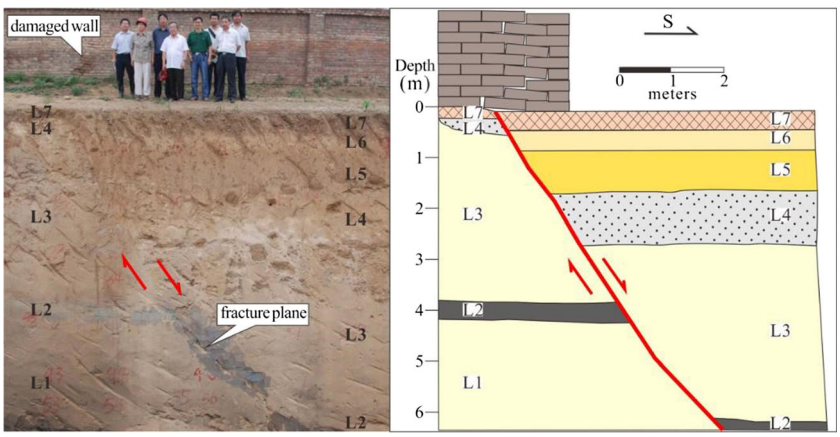


**Fig. 7** An exploratory trench in the Xiwanglu village (modified from the Beijing Hydrogeological and Engineering Geological Survey 2007). Location is shown in Fig. 4. L1, L3, L5, and L6 is silty clay, L2 is organic clay, L4 is sand, and L7 is fill

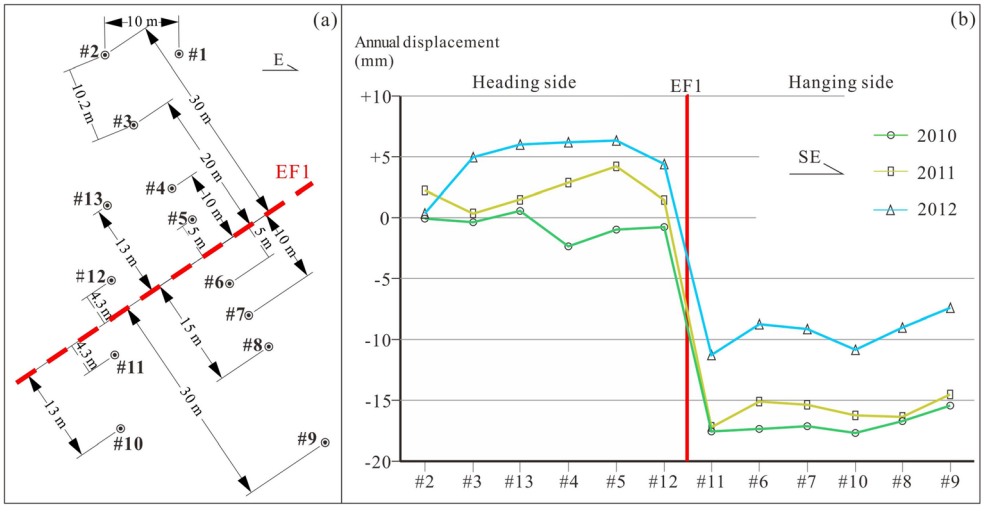


**Fig. 8** Layout and annual vertical displacement of the observation points (derived from the Beijing Hydrogeological and Engineering Geological Survey 2014). **a** Locations of all of the observation points. **b** Annual displacement of the twelve observation points in 2010, 2011, and 2012; "+" indicates uplift and "-" indicates subsidence

According to our investigation, all of the structures of the Beijing 2nd rubber plant were demolished in the late 2000s and no further observations on the fissures at this site. Similar to the EF1 fissures, the cracks and identical subsidence pattern of the EF2 fissures were found from the Shunyi petroleum company (Fig. 11) to the Wujiaying village.

In 2017, we noticed the appearance of a large numbers of earth fissures at the Beijing Capital International Airport (BCIA), which were not reported before. According to the unpublished records from the airport, an unprecedented number of cracks and vertical offsets both occurred in the airstrips, taxiways, underground passages, aprons, Terminal 2, and Terminal 3. As a result, the infrastructure was damaged to a certain degree, and nearly 10% of the total airport area was affected. Satellite images (Figs. 12a–f) indicate that the fissures mainly emerged along a NE-SW trend in the concrete near the Terminal 2, beginning in 2009. Figure 12f shows that repair and preventative efforts did not prevent the fissures from propagating. In our subsequent survey, for the first time, identical geological phenomena were discovered from the Air China hotel (Fig. 13) to the Wuyuan logistic park (Fig. 14). The Wuyuan logistic park is very close to the SHF (Fig. 2), and no fissures or damages have been observed or reported on the other side of this regional normal fault until now.

The EF2 fissures, which extend for 13 km nearly, discontinuously appeared from downtown Beijing to the Shunyi District, along a broad N30 °~60 °E trend approximately parallel to the EF1 fissures. The statistics (Table 3) also show that the differential subsidence generally occupies the first place and this deformation pattern is similar to the EF1 fissures. In addition, the lengths and the vertical dislocations of the southern segment of the EF2 fissures, from the BCIA to the

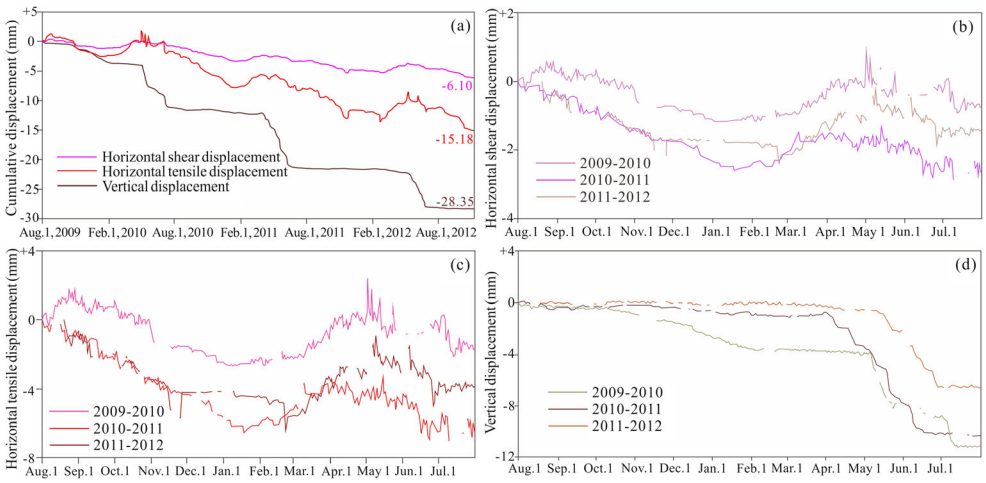


**Fig. 9** Relative displacement curves for the hanging wall in 2009-2012 (derived from Wang et al. 2013). **a** cumulative horizontal and vertical displacements in 3 years. For the horizontal shear displacement "+" indicates left-lateral and "-" indicates right-lateral, for the horizontal tensile displacement "+" indicates compression and "-" indicates tension, and for the vertical displacement "+" indicates uplift and "-" indicates subsidence. **b** Annual horizontal shear displacement curves. **c** Annual horizontal tensile displacement curves. **d** Annual vertical displacement curves

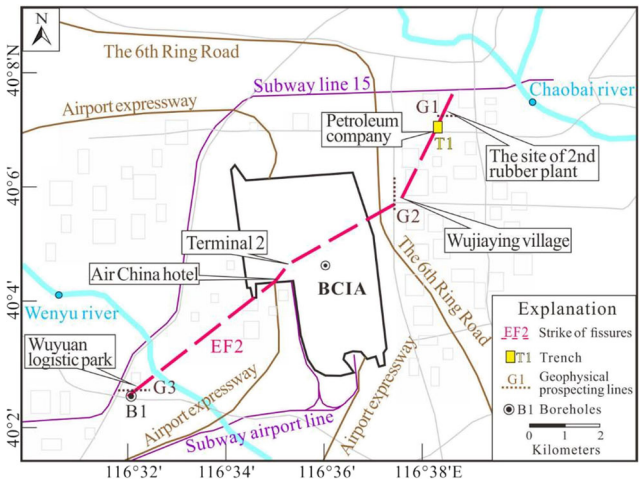


**Fig. 10** Location of the EF2 fissures and the associated trench, geophysical prospecting lines, and boreholes (assembled from the Beijing Hydrogeological and Engineering Geological Survey 2007 and this paper)

Wuyuan logistic park, are an order of magnitude larger than that of the northern segment, from the Beijing 2nd rubber plant to the Wujiaying village. This indicates that the geologic conditions in the southwestern side of the study area are more favorable for earth fissure formation and growth.

The Beijing Hydrogeological and Engineering Geological Survey (2007) used an E-W trending trench in the petroleum company and several GPR prospecting lines close to the 2nd rubber plant and Wujiaying village to explore the shallow geometric structures of the northern segment of the EF2 fissures, revealing that the earth fissures formed above a preexisting regional fault, i.e., the SYF. In Fig. 15, a high-angle fault was discovered at a depth of 4 m, dislocating the subsurface layers deposited in 20.7 ± 1.7 ka-24.1 ± 2.5 ka B.P., according to the dating results from the Beijing Hydrogeological and Engineering Geological Survey (2007). The high-angle fracture plane is believed to be an extension of the SYF.

We intended to excavate trenches to explore the southern segment of the EF2 fissures, but excavation is forbidden in the vicinity of the BCIA and was explicitly rejected by the owner of the Wuyuan logistic park. Thus, we choose the geophysical prospecting and drilling instead. Geophysical prospecting lines in front of the southern wall of the Wuyuan logistic park revealed a spatial relationship between the surface deformation and the preexisting faults beneath the surface. Figure 16a shows the SYF beneath the damaged wall dislocated $Qp_1$~$Qp_3$. As for the upper layers, the relationship is not clear due to the low veracity and precision of this physical prospecting techniques. Figure 16b shows a clearer image that the 1~8-m-deep layers under the damaged wall have been dislocated by a normal fault, which is inferred as an extension from the SYF. The fault is only covered by the newly covered hardened fills (less than 1 m thick) and is close enough to the damaged wall. Descriptions of the shallow boreholes (Fig. 16c), i.e., B1, verified the position of the fault plane beneath the damaged wall.

## Characteristics of the EF3 fissures

The origin of the EF3 fissures can be traced back to the Tangshan earthquake, when the buildings and roads cracked with small or tiny vertical offsets and the sands boiled along the bank of the Chaobai River (Beijing Hydrogeological and Engineering Geological Survey, 2007). The damaged structures had been repaired or rebuilt. However, new fissures emerged occasionally over the next few decades, despite no more seismic effects occurred. Based on current observations, the new EF3 fissures are small, disorganized, and confined to several suburban communities in the Shunyi district, from Beixiaoying town to Nancai town (Fig. 17). The fissures have been observed in Maxinzhuang village, Qiaotou village, Huangjiachang village, and Daoxianzhuang village by the Beijing Hydrogeological and Engineering Geological Survey (2007), and our survey extended the scope to the south.

From our observation, the EF3 fissures are scattered along the left bank of the Chaobai River with small and discrete


**Fig. 11** Earth fissure and damaged structures in the Shunyi petroleum company. Photos were taken on July 2, 2018. Location is shown in Fig. 10. **a** Southeastern side has subsided. **b** Six-meter-long earth fissure trending N15°E


**Fig. 12** Cracked cement concrete slabs and subsided southeastern side in the BCIA. Fissures are 300-m long, 1~10-cm wide, and have 1~12-cm vertical dislocations. Location is shown in Fig. 10. **a~f** Pictures are based on Google Earth image. **g~h** Photos were taken on March 15, 2017

cracks, without vertical offsets nearly. This distinctly different distribution and damage patterns indicate that the EF3 fissures are not extensions of the EF1 fissures but were formed by another mechanism. Statistics (Table 4) demonstrate that the formation of the EF3 fissures was not influenced by the regional normal fault, unlike the EF1 and EF2 fissures, despite the SYF is buried beneath this area as well (shown in Fig. 2).

The EF3 fissures presented a formation pattern following bending beam model, which has been discussed by Jachens and Holzer (1982), Budhu (2008, 2011), Hernandez-Marin and Burbey (2010), and Xu et al. (2019). In this theory, vertical or inclined V-shaped cracks opened at the top and propagated downward, mainly under tensile stresses. Typical examples can be observed in Beicai village where two groups of

**Fig. 13** Damaged pavement in a garden of the Air China hotel. Photos were taken on June 8, 2018. Location is shown in Fig. 10. Twenty-five-meter-long earth fissures trending N40°E. Southeastern side has subsided 10~30 cm

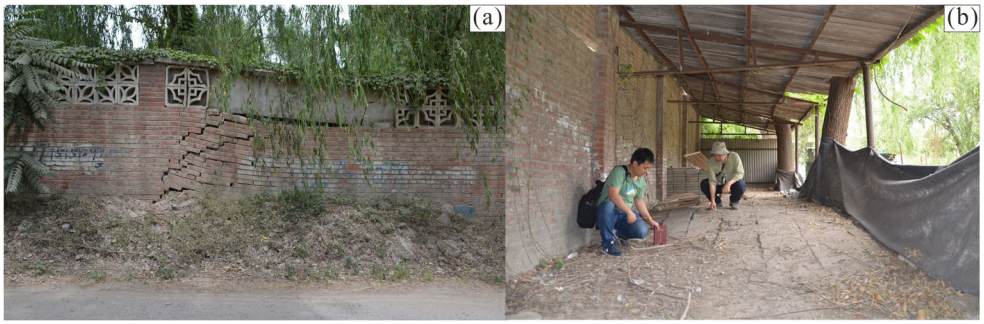


**Fig. 14** Damages in the Wuyuan logistic park. Photos were taken on June 2, 2017. Location is shown in Fig. 10. Three-hundred-meter-long earth fissures trending N30 °~40 °E in the Wuyuan logistic park. Southeastern side has subsided 10~20 cm. Differential subsidence and earth fissure occurred starting in about 2010, based on interviews. **a** Damaged southern wall. **b** Damaged southern wall and subsided ground surface

fissures (Fig. 18 and Fig. 19), which are almost perpendicular to each other in the horizontal direction (Fig. 17), cracked houses and infrastructures. Figure 19 shows an inverted "Y" type fissure formed along the weak planes between a wall and a dike by bending. The upper branch of the fissure caused the wall to tilt and the lower branch damaged a drain pipe.

## Discussion

The EF1, EF2, and EF3 fissures formed close to each other, in the northeastern Beijing Plain. Despite of their similar climates, topography, and tectonics, the characteristics of the three fissure zones are different. The EF1 and EF2 fissures are long and linear in the horizontal direction, and their distributions are closely associated to the regional normal faults HGF and SYF, respectively. By contrast, the EF3 fissures are absolutely not. This most likely indicates different fissure formation processes, which are controlled by the internal and external factors within the northeastern Beijing Plain. Based on the spatial distribution, deformation patterns and dynamic responses of the EF1, EF2, and EF3 fissures, the major factors involved in their formation include (a) preexisting faults, (b) paleochannels, and (c) pumping.

### Preexisting faults

Regional preexisting faults are a considerable geological factor in earth fissure formation due to fault movements (Pampeyan et al. 1988; Ayalew et al. 2004; Budhu and Adiyaman 2012; Peng et al. 2016; Loli et al. 2018). In addition, numerical simulations performed by Sheng et al. (2003) and Hernandez-Marin and Burbey (2009, 2010) demonstrated that the regions surrounding the crack tips of preexisting faults, where energy and stress are concentrated, are vulnerable to fracturing after groundwater pumping.

In the northeastern Beijing plain, preexisting faults played a crucial role in the formation of the EF1 and EF2 fissures. The distribution and deformation patterns of the EF1 and EF2 fissures are consistent with segments of the HGF and SYF, respectively. The two faults have propagated upward into the shallow sediments, or even to the ground surface, which are shown in excavated trenches (Figs. 7 and 15) and geophysical prospecting profiles (Fig. 16). The deposits around the crack tips of these shallowly buried faults are fragile and sensitive; this explains why there is a lot of overlaps between the two groups of earth fissures and the preexisting faults in the horizontal direction. Second, the kinematic consistency between the preexisting faults and the earth fissures confirms the definite control action of the two normal faults. The dip-slip movements of the HGF and SYF were dominated by vertical displacements in the Quaternary period, which are identical to the monitoring results for the EF1 fissure shown in Fig. 9 and the damage pattern caused by the EF2 fissures shown in Fig. 13 and Fig. 14.

The activity and kinematics of the preexisting faults are controlled by the tectonic stress field in North China, which was induced by the subduction of the Pacific Plate and the

**Table 3** Statistics for the EF2 fissures (assembled from the Beijing Hydrogeological and Engineering Geological Survey 2007 and this paper)

| Location of EF2 | Strike | Length (m) | Width (cm) | Vertical dislocation (cm) |
|---|---|---|---|---|
| The 2nd rubber plant | N12 °~90 °E | 270 | < 9 | 1~7 |
| Petroleum company | N15 °~40 °E | 40 | < 2 | 1~2 |
| Wujiaying village | N40 °~45 °E | 10 | < 3 | 1~2 |
| BCIA | N40 °~75 °E | 900 | < 10 | 1~12 |
| Air China hotel | N30 °~60 °E | 200 | < 2 | 10~30 |
| Wuyuan logistic park | N30 °~40 °E | 300 | < 5 | 10~20 |

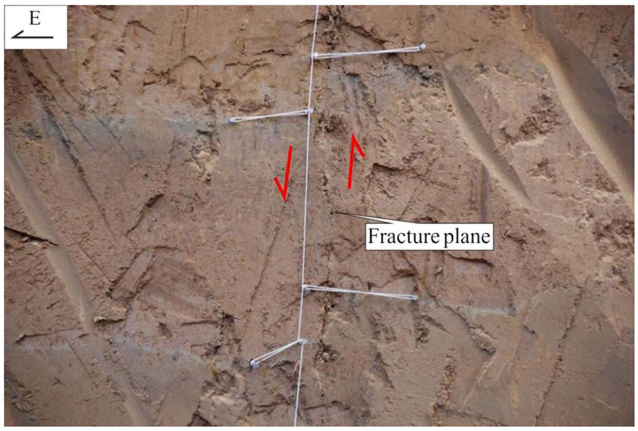


**Fig. 15** Part of a trench in the Shunyi petroleum company showing that the brown clays and gray silts, at a depth of 4~5 m, have slipped down along a preexisting fracture plane (derived from the Beijing Hydrogeological and Engineering Geological Survey 2007). Vertical dislocation was 14 cm. Location is shown in Fig. 10

Philippine Sea Plate, as well as the Indian-Eurasian collision. Cui et al. (2010) determined that the mean orientation of the current regional maximum compressive horizontal stress ($SH_{max}$) is NEE-SWW, in North China, by analyzing the focal-mechanism solutions of thousands of moderate and small earthquakes. Qin et al. (2014) measured the in situ stress using hydraulic fracturing, determining that the $SH_{max}$ orientation is N81 °~82 °E at a depth of about 400 m in downtown Beijing, and N79 °~66 °W at depths of 100~400 m in the Miyun District. The results indicate that the current tectonic stress field in the southwestern part of the study area is represented by NEE-SWW horizontal compressive stress and NNW-SSE horizontal tensile stress, while in the northeastern part it is represented by NWW-SEE horizontal compressive stress and NNE-SSW horizontal tensile stress. Thus, the orientation of the horizontal compressive stress and tensile stress rotates clockwise from southwest to northeast. The NNW-SSE-oriented tensile stress in the southwestern part of the study area induced the activity on the HGF and SYF and facilitated the initiation of the EF1 and EF2 fissures in the fragile regions above the preexisting faults, but the NNE-SSW-oriented tensile stress in the northeastern part did not (shown in Figs. 1 and 2).

## Paleochannel

Paleochannels contribute to earth fissure formation, in which heavy rainfall, shaking or earthquakes, and groundwater pumping are commonly implicated (Pacheco-Martínez et al.

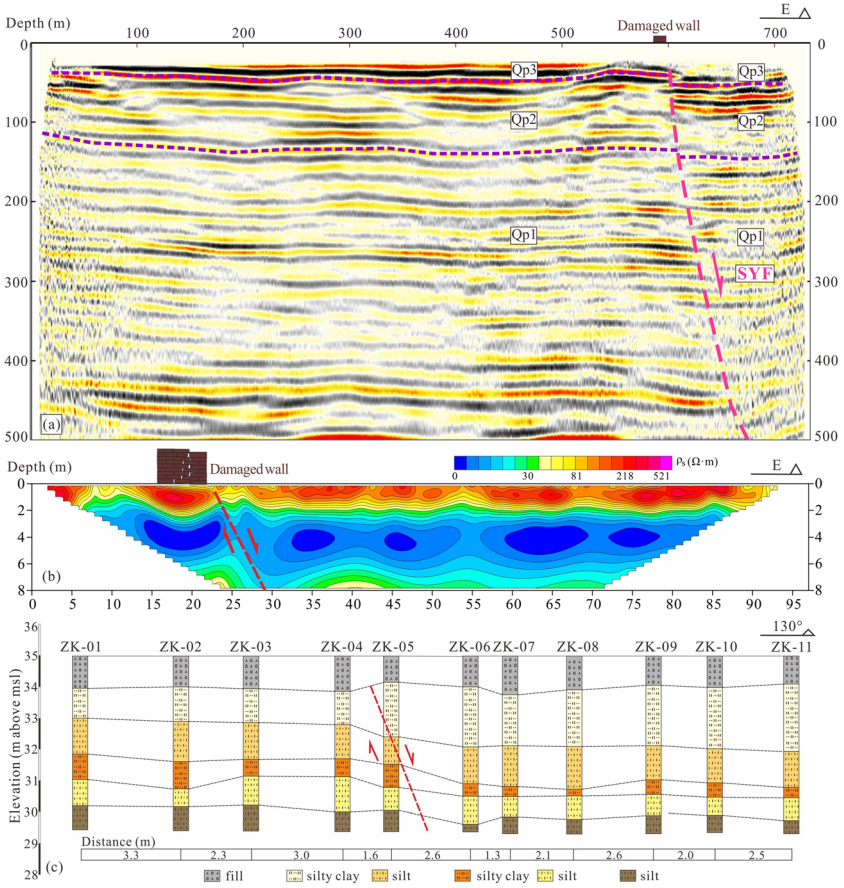


**Fig. 16** Geophysical prospecting profiles on the pavement, outside the damaged southern wall of the Wuyuan logistic park, and shallow boreholes in the wasteland about 200 m south of the geophysical prospecting profiles. Locations are shown in Fig. 10. **a** Seismic prospecting profile. **b** Resistivity prospecting profile. **c** Geological section based on the shallow boreholes

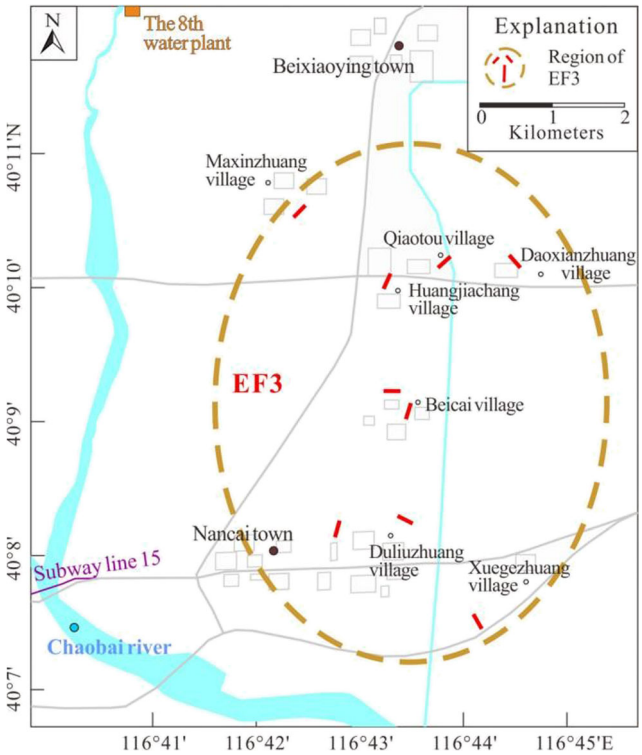


**Fig. 17** Location of the EF3 fissures (assembled from the Beijing Hydrogeological and Engineering Geological Survey 2007 and this paper)

2013; Gaur et al. 2015). Instability and resultant uneven settlement are prone to occur due to the heterogeneity, anisotropism, and loose structures of shallowly buried paleochannel deposits. It results in the earth fissure formation, and piping, surface erosion, and human activity accelerate this process.

The Chaobai River, which is the second largest river in Beijing, flooded and avulsed frequently in the late Pleistocene and Holocene, despite the significant decrease in flow after the 1950s due to continued dry weather and the impoundment of the Miyun reservoir in the upper streams (Yu et al. 2013). The courses of the river changed, and the paleochannels formed accordingly during the geological ages. Heterogeneous sands and gravels delivered by floods were deposited along the paleochannels at various depths (Fig. 2).

The paleochannel provided a favorable setting for the formation of the EF3 fissures. The distribution of the EF3 fissures is not controlled by the buried regional fault, unlike the EF1 and EF2 fissures. In contrast, they form roughly trending N-S, approximately following the margins of the shallowly buried paleochannels of the Chaobai River, which is verified by the D03 and D04 descriptions (Fig. 2). In addition, earth fissures associated with paleochannels have short lengths and shallow depths in general (Pacheco-Martínez et al. 2013; Xu et al. 2019), which agrees with our findings for the EF3 fissures (Table 4).

Additionally, the formation pattern of earth fissures on the margins of paleochannels follows the bending model (Pacheco-Martínez et al. 2013; Xu et al. 2019). In the northeastern Beijing Plain, there are two basic layers consisting of a stiff layer, i.e., concrete and hardened fills, and a compressible layer, i.e., heterogeneous paleochannel deposits. As soon as uneven vertical deformation occurs in the compressible layer, the upper stiff layer bends and cracks above the voids due to the gravitational stress and additional stresses. This pattern is exhibited by the EF3 fissures (Figs. 18 and 19).

## Pumping

Pumping-induced earth fissures have been reported in many countries (Jachens and Holzer 1982; Pampeyan et al. 1988; Budhu 2011; Pacheco-Martínez et al. 2013; Zhang et al. 2015; Miller et al. 2017). Differential compaction of a heterogeneous unconsolidated aquifer system caused by drawdown from excessive groundwater extraction is considered to be the main reason for earth fissure formation. Drawdown increases the effective stress in the aquifer system, resulting in an impermanent and permanent compaction.

Pumping also triggers partial aseismic reactivation of preexisting normal faults, which is represented by the relative subsidence of the hanging wall and the resultant earth fissures. This earth fissure formation mechanism can be explained by the differential horizontal movement of the aquifers and the rotation of the fracture plane, which is driven by horizontal hydraulic forces induced by groundwater pumping (Helm 1994; Budhu 2008; Hernandez-Marin and Burbey 2009, 2010).

**Table 4** Statistics for the EF3 fissures (assembled from the Beijing Hydrogeological and Engineering Geological Survey 2007 and this paper)

| Location of EF3 | Strike | Length (m) | Width (cm) | Vertical dislocation (cm) |
|---|---|---|---|---|
| Maxinzhuang village | NE-SW | < 5 | < 4 | < 1 |
| Qiaotou village | NE-SW | < 5 | < 3 | < 1 |
| Daoxianzhuang village | NW-SE | 5 | < 3 | < 1 |
| Huangjiachang village | NE-SW | < 5 | < 2 | < 1 |
| Beicai village | E-W/NE-SW | 10~20 | < 3 | < 2 |
| Duliuzhuang village | NW-SE/NE-SW | 10~25 | < 5 | < 2 |
| Xuegezhuang village | NW-SE | < 5 | < 1 | < 1 |

**Fig. 18** Cracked house and pavement, without a measurable vertical offset, in Beicai village. Photos were taken on May 16, 2018. Location is shown in Fig. 17. Fissures in the pavement, trending E-W, 10~20-m long

In the northeastern Beijing Plain, pumping is inferred to be an immediate trigger of the earth fissure formation. According to the automatic monitoring data for the EF1 fissures (Fig. 9), the relative vertical displacement of the hanging wall experienced abrupt seasonal (April–June or May–July) changes over 3 successive years (2010–2012) without seismic events, indicating that the differential subsidence cannot be attributed to tectonics. Disturbance from heavy rainfall can be excluded from consideration as well, because the rainy season in Beijing occurred in June–September in 2010–2012, not in April–June or May–July, based on the public records from the China Meteorological Administration. Hence, pumping is concluded to be the exclusive cause.

In addition, in Fig. 9, horizontal compression and horizontal left-lateral shear, indicating a north-trending movement of the hanging wall of the EF1 fissures, occurred synchronously with each sharp vertical displacement, while the horizontal displacements returned as soon

**Fig. 19** Cracked house, wall, and dike with small vertical offsets in Beicai village. Photos were taken on May 16, 2018. Location is shown in Fig. 17. Fissures trending N10°E mostly covered by new concrete pavement. Wall tilted inward by fissure propagation

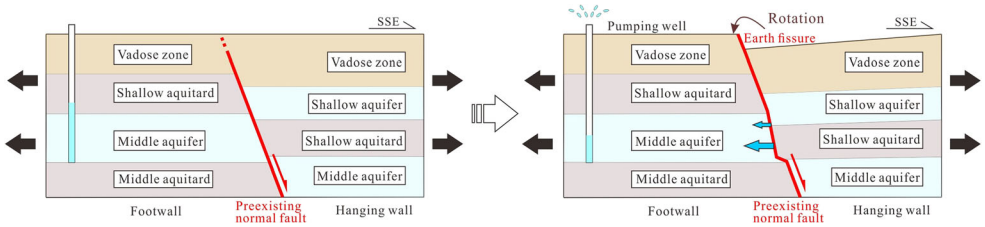


**Fig. 20** Conceptual model for pumping-induced earth fissures on the presence of a preexisting normal fault. The black arrows indicate the orientations of regional tensile horizontal stress. The blue arrow indicates the orientation of the horizontal hydraulic driving forces induced by pumping

as the sharp vertical displacement ceased. A reasonable explanation for the earth fissure formation is presented. Part of the hanging wall of the HGF was forced to slip downward with a north-trending movement in response to the sudden increase in groundwater pumping after each winter ended to meet the forthcoming peak water demand. This resulted in the abrupt propagation of the HGF and the formation of the EF1 fissures. No more clear subsidence of the hanging wall occurred after each rainy season coming probably because the decline in groundwater table was reversed by the rainfall recharge. Besides, the shear strength between the fault plane was reduced because of the horizontal displacement of the aquifers. It stimulates the activity of the preexisting fault and accelerates the slip process on the hanging wall. This hypothetical formation mechanism is possible for the EF2 fissures as well, considering the similar structures between the HGF and SYF.

Regarding the formation of the EF3 fissures, the role of pumping is clearer. The Beijing 8th water plant established along the left bank of the Chaobai River (Fig. 3a) extracted an enormous amount of groundwater. As a result, the groundwater table declined, and the depression cone expanded. Beixiaoying town and Nancai town were affected as shown by the monitoring data of wells M1, M2, and M3 (Fig. 3). The effective stress increased in response to the reduction of pore water stress accompanying drawdown, leading to a compaction of the rapidly deposited sediments in the shallowly buried paleochannel of the Chaobai River. Due to the heterogeneity and anisotropism of the deposits, differential subsidence occurred, and the upper stiff layers cracked by bending mechanism subsequently, particularly above the margins of the buried paleochannel.

## Earth fissure formation process

Preexisting faults, paleochannels, and pumping are the main causes for the EFBP fissures formation. It is concluded that the preexisting faults and paleochannels provided favorable settings for the fissure initiation. The fragile regions surrounding the crack tips of the preexisting faults are vulnerable to fracturing because energy and stress concentrate on these locations given a suitable current tectonic stress field and strong external interference. As for paleochannels, earth fissures occur accompanying the uneven settlements frequently due to the heterogeneity, anisotropism, and loose structures of shallowly buried paleochannel deposits. It is also concluded that the groundwater pumping triggered the EFBP fissures formation and deformation. Excessive groundwater extraction causes a decline in groundwater table, which induced regional differential compaction of the unconsolidated deposits. In addition, the pumping provides a horizontal hydraulic driving force pointing to the pumping wells to activate the preexisting normal faults and cause new fractures formation.

Thus, the formation of the EFBP fissures was induced by the groundwater pumping, and the formation processes can be classified into two categories: (1) on the existence of preexisting normal faults and (2) on the existence of paleochannels. Two hypothetical conceptual models (Figs. 20 and 21) are presented to illustrate these formation processes.

Figure 20 shows a conceptual model for pumping-induced earth fissures on the presence of a preexisting normal fault. The buried normal fault trends NE-SW, dips southeast. Under an extensional stress field, it develops and propagates slowly to the ground surface. This fault model is in agreement with the HGF and the SYF. The characteristics of the two faults are

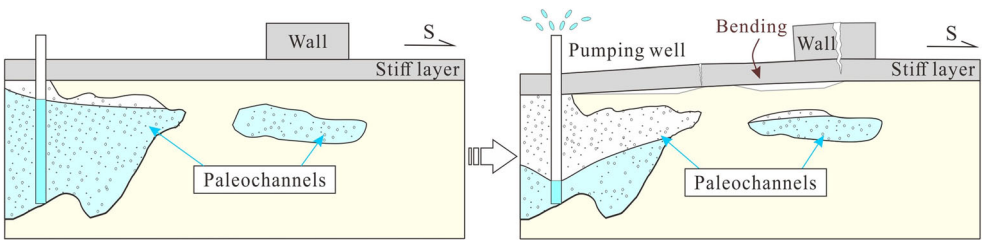


**Fig. 21** Conceptual model for pumping-induced earth fissures on the presence of paleochannels

shown in Table 1, and the tectonic stress field has been determined by Cui et al. (2010) as well as by Qin et al. (2014) and is discussed in this paper. When the well starts pumping, the horizontal hydraulic forces are generated within the aquifer, which cause the horizontal differential movements of the soil particles and preexisting fracture plane. The movements leave voids in the exploited aquifer along the fracture plane, which trend to be filled up by the upper soil layers in the hanging wall. Accordingly, under the extensional stress field, the hanging wall slips downward abruptly with an anticlockwise rotation and the earth fissures form. The deformation pattern is shown in the excavated trench (Fig. 7) and geophysical prospecting profiles (Fig. 16), and the earth fissure formation process is supported by the monitoring data (Fig. 9), for the EF1 and EF2 fissures.

Figure 21 shows a conceptual model for pumping-induced earth fissures on the presence of paleochannels. The paleochannels are buried at shallow depths near the current river channel, based on the regional geological map and the drill-hole columns in the Chaobai River (Fig. 2). The groundwater flows southward, until the long-term large-scale groundwater exploitation. The directional changes of the groundwater flows are in accordance with the monitoring data for the fluctuations of the groundwater levels near to the Beijing 8th water plant (Fig. 3). The drawdown caused by the overextraction of groundwater induced the regional compaction of paleochannel deposits and the localized differential subsidence. Once the failure of the stiff layer occurs, the cracks initiate at the top and propagate downward by the bending beam mechanism. This earth fissure formation patterns are observed in the EF3 fissures (Figs. 18 and 19).

## Conclusion

The EF1, EF2, and EF3 fissures, located in the northeastern Beijing Plain, damaged numerous houses, roads, and infrastructures and will likely continue to cause damage in the future. Based on ground surveys, drilling, geophysical prospecting, satellite images, and the records in literature, the characteristics and main causes of the EFBP fissures were determined in this study.

The EF1 and EF2 fissures, which have large vertical offsets and small widths, formed in several places along certain segments of the NE-SW trending regional normal faults, the HGF and SYF, respectively. The deformation patterns of the EF1 and EF2 fissures are characterized by consistent subsidence on the southeastern side. Trenches and geophysical prospecting profiles were used to determine that the EF1 and EF2 fissures propagated from the HGF and SYF, respectively. Based on the monitoring data for the EF1 fissures, it is concluded that the formation and deformation of the EFBP fissures occurred in response to drawdown caused by the groundwater pumping.

The EF3 fissures are not associated with the adjacent preexisting fault, i.e., the SYF, but are distributed following the paleochannel of the Chaobai River in a N-S trending, which is roughly parallel to the current channel. The distinction of the EF3 fissures is represented by V-shaped cracks with short lengths and negligible vertical offsets. The formation of the EF3 fissures is based on the bending mechanism which caused the cracks open at the top of a stiff layer and propagate downward to a shallow depth.

Three major factors, i.e., preexisting faults, paleochannels, and pumping played different roles in the EFBP formation. The preexisting faults and paleochannels provided favorable settings for the fissure initiation, and the groundwater pumping triggered the EFBP fissures formation and deformation. Thus, the formation processes of the EFBP fissures can be classified into two categories: (1) on the existence of preexisting normal faults and (2) on the existence of paleochannels.

**Acknowledgments** The authors are thankful to the Beijing Hydrogeological and Engineering Geological Survey for providing valuable data. The authors are also grateful to the editor-in-chief and the reviewers for the constructive comments which helped in improving our paper.

**Funding information** This research was funded by the China Geological Survey (Grant No. DD20160267, DD20190317).

## References

Al Fouzan F, Dafalla MA (2013) Study of cracks and fissures phenomenon in Central Saudi Arabia by applying geotechnical and geophysical techniques. Arab J Geosci 7(3):1157–1164

Ayalew L, Yamagishi H, Reik G (2004) Ground cracks in Ethiopian Rift Valley: facts and uncertainties. Eng Geol 75(3–4):309–324

Beijing Hydrogeological and Engineering Geological Survey (2007) Preliminary regional engineering geological exploration report in Shunyi new town, Beijing. Unpublished report (in Chinese)

Beijing Hydrogeological and Engineering Geological Survey (2014) Special exploration report on subsidence, earth fissures in Beijing-Shenyang passenger dedicated railway (Beijing section). Unpublished report (in Chinese)

Budhu M (2008) Mechanics of earth fissures using the Mohr-Coulomb failure criterion. Environ Eng Geosci XIV(4):281–295

Budhu M (2011) Earth fissure formation from the mechanics of groundwater pumping. Int J Geomech 11(1):1–11

Budhu M, Adiyaman I (2012) Earth fissure formation from groundwater pumping and the influence of a stiff upper cemented layer. Q J Eng Geol Hydrogeol 45(2):197–205

Chiaradonna A, Tropeano G, d'Onofrio A, Silvestri F (2019) Interpreting the deformation phenomena of a levee damaged during the 2012 Emilia earthquake. Soil Dyn Earthq Eng 124:389–398

Conway BD (2015) Land subsidence and earth fissures in south-central and southern Arizona, USA. Hydrogeol J 24(3):649–655

Cui X, Xie F, Li R, Zhang H (2010) Heterogeneous features of state of tectonic stress filed in North China and deep stress in coal mine. Chin J Rock Mech Eng 29(supp.1):2755–2761 (in Chinese)

De Filippis L, Faccenna C, Billi A, Anzalone E, Brilli M, Ozkul M, Soligo M, Tuccimei P, Villa IM (2012) Growth of fissure ridge travertines from geothermal springs of Denizli Basin, western Turkey. Geol Soc Am Bull 124(9–10):1629–1645

Foster S, Garduno H, Evans R, Olson D, Tian Y, Zhang W, Han Z (2004) Quaternary aquifer of the North China plain - assessing and achieving groundwater resource sustainability. Hydrogeol J 12(1):81–93

Gaur VP, Kar SK, Srivastava M (2015) Development of ground fissures: a case study from southern parts of Uttar Pradesh, India. J Geol Soc India 86(6):671–678

Ghazifard A, Moslehi A, Safaei H, Roostaei M (2016) Effects of groundwater withdrawal on land subsidence in Kashan plain, Iran. Bull Eng Geol Environ 75(3):1157–1168

Guo H, Zhao J (2018) The surface rupture zone and paleoseismic evidence on the seismogenic fault of the 1976 Ms 7.8 Tangshan earthquake, China. Geomorphology 327:297–306

Helm DC (1994) Hydraulic forces that play a role in generating fissures at depth. Bull Assoc Eng Geol 31(3):293–304

Hernandez-Marin M, Burbey TJ (2009) The role of faulting on surface deformation patterns from pumping-induced groundwater flow (Las Vegas Valley, USA). Hydrogeol J 17(8):1859–1875

Hernandez-Marin M, Burbey TJ (2010) Controls on initiation and propagation of pumping-induced earth fissures: insights from numerical simulations. Hydrogeol J 18(8):1773–1785

Hernandez-Marin M, Pacheco-Martínez J, Burbey TJ, Carreón-Freyre DC, Ochoa-González GH, Campos-Moreno GE, de Lira-Gómez P (2017) Evaluation of subsurface infiltration and displacement in a subsidence-reactivated normal fault in the Aguascalientes Valley, Mexico. Environ Earth Sci 76(24):812

Jachens RC, Holzer TL (1982) Differential compaction mechanism for earth fissures near Casa Grande, Arizona. Geol Soc Am Bull 93(10): 998–1012

Jiao Q, Qiu Z, Fan G (2005) Analysis on recent tectonic activity and seismicity of Babaoshan-Huangzhuang-Gaoliying fault in Beijing region. J Geod Geodyn 25(4):50–54 (in Chinese)

Li SR, Santosh M (2014) Metallogeny and craton destruction: records from the North China Craton. Ore Geol Rev 56:376–414

Li Y, Gong H, Zhu L, Li X, Wang R, Guo G (2017) Characterizing land displacement in complex hydrogeological and geological settings: a case study in the Beijing plain, China. Nat Hazards 87(1):323–343

Loli M, Kourkoulis R, Gazetas G (2018) Physical and numerical modeling of hybrid foundations to mitigate seismic fault rupture effects. J Geotech Geoenviron 144(11):04018083

Lu Q, Peng J, Deng Y, Li L, Feng L (2014) Failure characteristics and influence width of Beiqijia-Gaoliying ground fissure in Beijing. Geotech Invest Survey 6:5–11 (in Chinese)

McDonald RI, Weber K, Padowski J, Flörke M, Schneider C, Green PA, Gleeson T, Eckman S, Lehner B, Balk D, Boucher T, Grill G, Montgomery M (2014) Water on an urban planet: urbanization and the reach of urban water infrastructure. Glob Environ Chang 27:96–105

Miller MM, Shirzaei M, Argus D (2017) Aquifer mechanical properties and decelerated compaction in Tucson, Arizona. J Geophys Res Solid Earth 122(10):8402–8416

Nábělek J, Chen WP, Ye H (1987) The Tangshan earthquake sequence and its implications for the evolution of the North China Basin. J Geophys Res 92(B12):12615

Nikbakhti O, Hashemi M, Banikheir M, Basmenj AK (2017) Geoenvironmental assessment of the formation and expansion of earth fissures as geological hazards along the route of the haram-to-haram highway, Iran. Bull Eng Geol Environ 77(4):1421–1438

Pacheco-Martínez J, Hernandez-Marín M, Burbey TJ, González-Cervantes N, Ortíz-Lozano JÁ, Zermeño-De-Leon ME, Solís-Pinto A (2013) Land subsidence and ground failure associated to groundwater exploitation in the Aguascalientes Valley, México. Eng Geol 164:172–186

Pampeyan EH, Holzer TL, Clark MM (1988) Modern ground failure in the Garlock fault zone, Fremont Valley, California. Geol Soc Am Bull 100(5):677–691

Peng J, Xu J, Ma R, Wang F (2016) Characteristics and mechanism of the Longyao ground fissure on North China plain, China. Eng Geol 214: 136–146

Pirajno F, Santosh M (2014) Rifting, intraplate magmatism, mineral systems and mantle dynamics in central-East Eurasia: an overview. Ore Geol Rev 63:265–295

Qi J, Yang Q (2010) Cenozoic structural deformation and dynamic processes of the Bohai Bay basin province, China. Mar Pet Geol 27(4): 757–771

Qin XH, Zhang P, Feng CJ, Sun WF, Tan CX, Chen QC, Peng YR (2014) In-situ stress measurements and slip stability of major faults in Beijing region, China. Chinese J Geophy 57(7):2165–2180 (in Chinese)

Qin H, Andrews CB, Tian F, Cao G, Luo Y, Liu J, Zheng C (2018) Groundwater-pumping optimization for land-subsidence control in Beijing plain, China. Hydrogeol J 26(4):1061–1081

Sheng ZP, Helm DC, Li J (2003) Mechanisms of earth fissuring caused by groundwater withdrawal. Environ Eng Geosci 9(4): 351–362

Wang H, Yang Y, Liu M, Jia S, Tian F (2013) Analysis of the activity of the Gaoliying ground fissure (Beijing), based on automatic monitoring. Shanghai Land Resour 34(2):64–67 (in Chinese)

Xu J, Peng J, An H, Wang F, Sun H, Hu H, Yang B (2019) Paleochannel-controlled earth fissures in Daming, North China plain and their implication for underground paleogeomorphology. Geomorphology 327:523–532

Yakubchuk AS (2009) Revised Mesozoic–Cenozoic orogenic architecture and gold metallogeny in the northern Circum-Pacific. Ore Geol Rev 35(3–4):447–454

Yang Y, Li GM, Dong YH, Li M, Yang JQ, Zhou D, Yang ZS, Zheng FD (2011) Influence of south to north water transfer on groundwater dynamic change in Beijing plain. Environ Earth Sci 65(4):1323–1331

Yu Y, Song X, Zhang Y, Zheng F, Liang J, Han D, Ma Y, Bu H (2013) Identification of key factors governing chemistry in groundwater near the water course recharged by reclaimed water at Miyun County, northern China. J Environ Sci 25(9):1754–1763

Zhang Y, Ma Y, Yang N, Shi W, Dong S (2003) Cenozoic extensional stress evolution in North China. J Geodyn 36(5):591–613

Zhang S, Nie G, Liu X, Ren J, Liu G (2005) Quaternary activities of northern segment of the Shunyi-Liangxiang fault. Earthq Res China 21(1):84–92 (in Chinese)

Zhang Y, Wang Z, Xue Y, Wu J, Yu J (2015) Mechanisms for earth fissure formation due to groundwater extraction in the Su-Xi-Chang area, China. Bull Eng Geol Environ 75(2):745–760

Zhang J, Fan J, Xu H (2016a) Research on the sustainable development measures of the underground water source area in Beijing. Urban Geology 11(1):99–104 (in Chinese)

Zhang L, He J, Bai L, Cai X, Wang J, Yang T (2016b) The response relationship between the variation characteristics of deposition rate of quaternary depression basin on the northern margin of Beijing depression and the activity of Shunyi fault. Geol China 43(2):511–519 (in Chinese)

Zhang X, Zhang L, Cai X, Bai L (2016c) A study of structure and activity characteristics of the northern segment of Huangzhuang-Gaoliying fault in Beijing plain area. Geol China 43(4):1258–1265 (in Chinese)

Zhang L, Bai L, Zhao Y, Zhang X, Yang T, Cai X, He F (2017) The difference of deposition rate in the boreholes at the junction between Nankou-Sunhe fault and Huangzhuang-Gaoliying fault and its response to fault activity in the Beijing area. Seismology and Geology 39(5):1048–1065 (in Chinese)

Zhou Y, Guo G, Zhang L, Cai X, Lei K (2016) The division of quaternary strata and tectonic evolution in Houshayu Sag of Beijing. Geol China 43(3):1067–1075 (in Chinese)

Zhu L, Gong H, Li X, Wang R, Chen B, Dai Z, Teatini P (2015) Land subsidence due to groundwater withdrawal in the northern Beijing plain, China. Eng Geol 193:243–255